The Free OD at the Air/D2O Interface Is Structurally and Dynamically Heterogeneous

ARTICLE *in* THE JOURNAL OF PHYSICAL CHEMISTRY B · SEPTEMBER 2013

Impact Factor: 3.3 · DOI: 10.1021/jp406577v · Source: PubMed

3 AUTHORS:

Yujin Tong
Fritz Haber Institute of the Max Planck Society
32 PUBLICATIONS **375** CITATIONS
SEE PROFILE

Ana Vila Verde
Max Planck Institute of Colloids and Interfaces
26 PUBLICATIONS **225** CITATIONS
SEE PROFILE

Richard Kramer Campen
Fritz Haber Institute of the Max Planck Society
37 PUBLICATIONS **1,228** CITATIONS
SEE PROFILE

THE JOURNAL OF PHYSICAL CHEMISTRY B

Article

pubs.acs.org/JPCB

The Free OD at the Air/D_2O Interface Is Structurally and Dynamically Heterogeneous

Yujin Tong,[†] Ana Vila Verde,[‡,¶] and R. Kramer Campen*[,†]

[†]Fritz Haber Institute of the Max Planck Society, Faradayweg 4-6, 14195 Berlin, Germany

[‡]Theory and Bio-Systems Department, Max Planck Institute of Colloids and Interfaces, Wissenschaftspark Golm, 14424 Potsdam, Germany

[¶]Physics Center, University of Minho, Campus de Gualtar, 4710-057 Braga, Portugal

Supporting Information

ABSTRACT: Air/water interfaces are both ubiquitous in the environment and technology and a useful model for hydrophobic solvation more generally. Previous experimental and computational studies have highlighted that molecular level markers of such an extended hydrophobic surface are broken hydrogen bonds and, as a result, OH groups that are not hydrogen bond donors: free OH. Understanding both the time-averaged structure and structural dynamics of these free OH thus plays a critical role in developing a quantitative, molecular level understanding of hydrophobic solvation. Here we show, by combining polarization-dependent vibrational sum frequency (VSF) spectroscopy and molecular dynamics simulation, that the free OD of D_2O at the air/D_2O interface is structurally and dynamically heterogeneous: that longer lived free OD groups tend to point closer to the surface normal, have a narrower orientational distribution, and are closer to the vapor phase. Knowledge of this structural heterogeneity should help link existing descriptions of hydrophobic solvation that focus either on the termination of the bulk hydrogen bond network or local density fluctuations. In addition the results of this study clarify that schemes to increase signal-to-noise ratios in VSF measurements by delaying the visible pulse relative to the infrared should be used only with independent constraints on the system's structural dynamics.

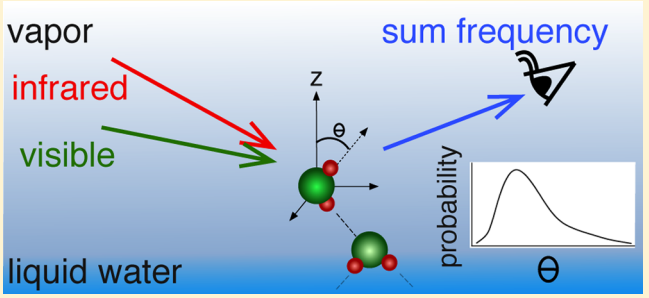

INTRODUCTION

Air/water interfaces are ubiquitous in the environment. Much work over the past several decades has clarified that understanding their molecular level structure is important in the quantitative description of processes such as the formation of marine aerosols, much heterogeneous atmospheric chemistry, and the development of lightning.[1,2] In parallel, much theoretical work has suggested that air is a model hydrophobic phase and that molecular structure at the air/water interface gives significant insight into the thermodynamics of hydrophobic solvation more generally.[3]

Because its frequency is a sensitive probe of the local hydrogen bonding environment,[4] in principle probing the OH stretch vibration of interfacial water can provide molecular level structural insight at the air/water interface. In practice, however, such measurements are challenging because conventional spectroscopies (infrared absorbance or spontaneous Raman) are not interface specific and the spectral response of interfacial water molecules is generally overwhelmed by the much larger number in the bulk. As initially demonstrated by Shen and co-workers, the laser-based technique vibrational sum frequency (VSF) spectroscopy is capable of overcoming these challenges.[5−7] In this technique, the output of pulsed infrared and visible lasers are overlapped spatially and temporally at an interface and the emitted field at the sum of the frequencies of the two incident beams is monitored. The sum frequency process is, by its symmetry selection rules, prohibited in media with inversion symmetry (within the dipole approximation), and there is thus no sum frequency emission from either bulk water or air. It is a spectroscopy because as the frequency of the infrared is tuned to a resonance of a molecule at the interface, emission increases by several orders of magnitude. Employing VSF spectroscopy, both the Shen group and subsequent investigators have recovered the spectral response of the OH stretch at the air/H_2O interface with interfacial specificity.[6−17]

This sum frequency OH stretch spectral response is a function of the polarization of the fields, the incident angles of the infrared and visible beams and the ensemble averaged orientation of the OH oscillators. As the *ssp* polarization condition (*s* polarized sum frequency, *s* polarized visible, and *p* polarized infrared, where *s* indicates polarization perpendicular and *p* polarization parallel to the plane of incidence) generates the largest signals in the hydrogen-bonded OH stretch under the majority of incident angles, most previous studies have been

Received: July 3, 2013
Revised: August 30, 2013
Published: September 3, 2013

   dx.doi.org/10.1021/jp406577v | *J. Phys. Chem. B* 2013, 117, 11753−11764

performed under these conditions. Such spectra typically show a broad double-peaked feature from 3100 to 3600 cm^{-1} and a single narrow peak at 3700 cm^{-1}.[6,7,11,16] While structural assignment of the lower frequency peak(s) has proven controversial,[18−22] the narrow high frequency peak has been unambiguously assigned to OH groups that point toward the vapor phase and do not donate a hydrogen bond: the *free* OH.

Subsequent VSF studies of various aqueous interfaces have found that this free OH spectral feature is present when water meets extended surfaces that are macroscopically hydrophobic but not when water meets surfaces that are macroscopically hydrophilic (where the macroscopic hydrophobicity of a surface can be quantified by, among a variety of techniques, the contact angle). For example, the free OH appears in the VSF OH stretch spectral response at the water/oil and water/hydrophobic self-assembled monolayer interfaces but not at the water/SiO_2.[23−25] Recently Ben-Amotz and co-workers have shown, in spontaneous Raman measurements, that free OH groups are also present in the solvation shell of alkanes larger than ∼1 nm in size.[26] Both the VSF and Raman measurements are consistent with previous theoretical and simulation studies that find the free energy of hydration of hydrophobic objects less than 1 nm is largely entropic in origin, that is, it does not require breaking a hydrogen bond, but that the free energy of solvation of hydrophobes greater than 1 nm in size is largely enthalpic in origin, that is, it requires hydrogen bond breaking.[3]

While the free OH spectral response is, in this sense, a molecular signature of solvation of a hydrophobic interface, it provides little insight into solvation thermodynamics. That is, the fact that a free OH spectral response can be observed provides little insight into why the free energy of wetting of hydrophobic surfaces may differ. Several decades of theory and simulation have found the statistics of local density fluctuations as a critical observable for this purpose.[3,27−33] Because the free OH VSF spectral response is a molecular level indicator of hydrophobicity, it thus seems reasonable to expect that this observable should be related to local density fluctuations. Elucidating this relationship requires understanding the structural heterogeneity and dynamics of the free OH and how these characteristics are related. We have recently quantified the rotational dynamics of the free OH at the air/water interface in a series of polarization-resolved infrared pump/VSF probe measurements and simulation.[34,35] This work strongly indicated that the free OH rotates approximately 3× more rapidly than OH in bulk H_2O and that the free OH has a characteristic time (τ_{reor}) of ∼850 fs before rotating toward bulk liquid to form a hydrogen bond. It also hinted at the possibility that the time averaged orientational distribution of free OH groups is lifetime-dependent. Subsequent computational studies by some of us, using fixed-charge classical all-atom simulations, indicated that as one moves away from bulk liquid H_2O toward the vapor, the angle of the free OH with respect to the surface normal (θ) decreases, the angular distribution narrows, and the lifetime (in the sense of the time required to rotate toward the liquid and form a hydrogen bond) increases[35] (the scenario suggested by this past work is summarized in Figure 1).

To date, a time-dependent change in the orientational distribution of the free OH has not been clearly demonstrated from VSF studies. As alluded to above, our previous work has clarified that the lifetime of the free OH of H_2O at the air/water interface before it rotates down to form a hydrogen bond in bulk is ∼850 fs.[34] Prior studies have shown that the VSF free

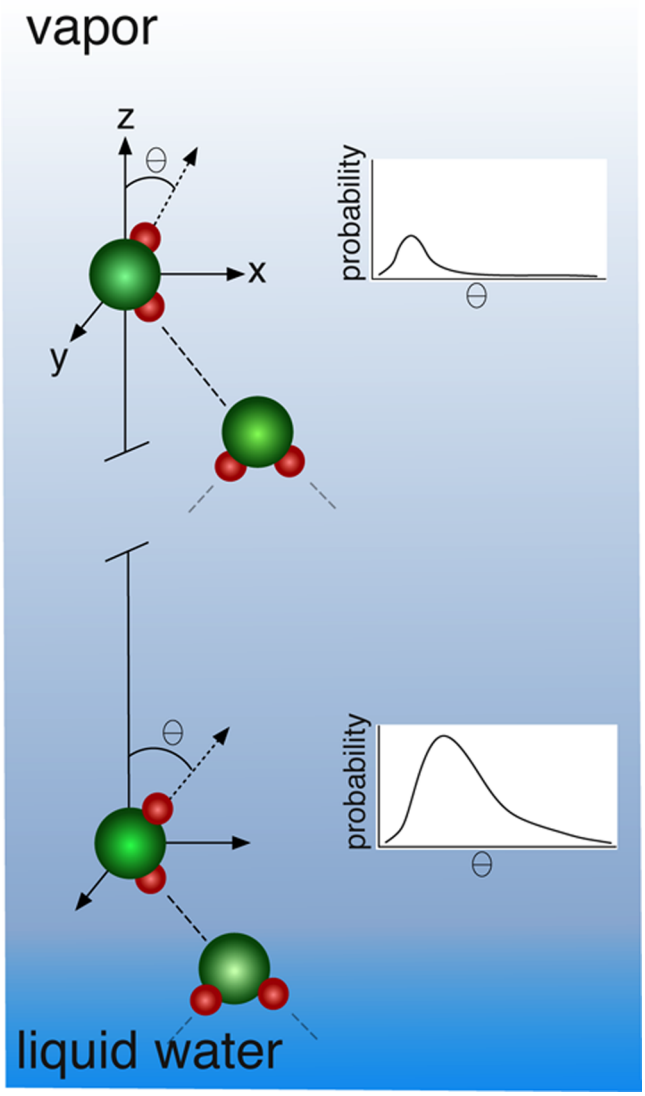

Figure 1. Prior IR pump/VSF probe measurements and classical all-atom molecular dynamics simulations[34,35] have suggested that as one moves from bulk liquid water to air free OH groups tend to point closer to the surface normal (i.e., smaller values of θ), have a narrower orientational distribution, and live longer before rotating down toward the bulk and forming a hydrogen bond.

OH spectral response (at the air/H_2O interface) can be well described by a Lorentzian with a damping constant (Γ) of 17 cm^{-1}.[12] This damping constant is equivalent to a dephasing time (T_2) of 310 fs ($2\pi c\Gamma = (1/T_2)$, where c = the speed of light). The fact that the characteristic rotation-induced lifetime of the free OH (τ_{reor}) is of order T_2 suggests that, if the lifetime-dependent orientational heterogeneity apparent in the simulation occurs in reality, we should be able to observe it by sampling the polarization-dependent static free OH VSF spectrum in the time domain.

In this study, then, we elucidate this lifetime-dependent change in orientational distribution experimentally and in simulation using the relevant free OH orientational distributions calculated from both the classical fixed charged water model SPC/E and the classical polarizable model SWM4-NDP. Both approaches lead to the same conclusion: as one samples at increasing times after the initial excitation, the average angle of the free OH with respect to the surface normal decreases and

dx.doi.org/10.1021/jp406577v | J. Phys. Chem. B 2013, 117, 11753−11764

the orientational distribution narrows. In conjunction with simulation this is shown to be the result of structural and dynamical heterogeneity: at longer times a long-lived subpopulation of free OH groups that is narrowed in orientational distribution and pointing closer to the surface normal than its brethren is sampled.

Our results have significant implications for the design and interpretation of VSF experiments. Recently, several authors have advocated delaying the visible pulse relative to the infrared as a means of increasing spectral resolution in VSF experiments.[36−38] We here show that for the free OH, and presumably for all local vibrational modes in materials in which structural dynamics occurs on time scales similar to vibrational dephasing and control vibrational relaxation, this approach is not advisable: such a temporal delay can lead to sampling different subpopulations of oscillators in a manner that cannot be understood without independent observables.

Prior studies of the air/water interface of some salt, acidic, and basic solutions have found that the spectral amplitude of the free OH decreased relative to that of pure water.[13,39,40] This observation has been interpreted as a time-averaged loss of population: OH groups that were, on average, free at the air/water interface have now rotated toward the liquid where they, on average, donate a hydrogen bond to either the interfacial solute or a water molecule. Our results suggest that by revisiting these measurements with the sort of time dependent polarization analysis we perform here, one might gain experimental insight into how far toward the vapor phase the solutes are distributed. In what follows we first discuss the methodological details of our experimental and computational approach, next the theoretical background necessary to analyze the VSF response, then our experimental and computational results and their implications and finally summarize our results and offer conclusions.

METHODS

Experimental Section. All simulations and experiments performed in this study involve the interrogation of the free OD of D_2O (and not the free OH of H_2O). This choice was made for technical reasons; our infrared source is more intense at 2730 than 3700 cm^{-1}. A large number of prior studies, both experimental and computational, have shown that, given the sum frequency spectral response of the OH stretch of H_2O one can quantitatively reproduce the measured sum frequency spectrum of the OD stretch of D_2O by scaling by the change in mass. Microscopic studies of the air/D_2O interface suggest (as we observe, see Supporting Information) that structural dynamics at the air/D_2O interface are slowed by ca. 10−20% from those at the air/H_2O interface, similar to the slowdown observed in bulk water.[41] As is discussed in more detail below, because the T_2 of the free OD of D_2O is also slightly longer than that of the free OH of H_2O, all conclusions from this work are expected to apply equally to the air/H_2O interface as well.

The VSF spectrometer used in this work has been described elsewhere.[42] In brief, the spectrometer consists of a mode-locked Ti:sapphire oscillator (Coherent Vitesse), a regenerative amplifier and a subsequent multipass amplifier (Quantronix Titan II) pumped by two Nd:YLF lasers (Quantronix 527 DP-H). The amplifier delivers 800 nm, 110 fs pulses at a repetition rate of 400 Hz; 2.5 mJ/pulse of the amplifier output is used to generate infrared pulses centered at 3650 nm (~2750 cm^{-1}) by difference frequency mixing of the signal and idler output of a commercial optical parametric amplifier (TOPAS, Light Conversion). The residual of the 800 nm light from the parametric amplification is spectrally narrowed using a homemade pulse shaper composed of a grating, mirror, and slit combination, and used as the up conversion field in the sum frequency process (i.e., the *visible* field in the usual VSF terminology). The temporal length of the visible pulse is controlled in this experiment by controlling the spectral width of the pulse emanating from the shaper. For all measurements the energy/pulse of the IR at the sample surface was 7.8, and that of the visible 15 μJ: the decrease in spectral width (and corresponding decrease in intensity) of the visible pulse is compensated by a $\lambda/2$ plate, polarizer, $\lambda/2$ plate sequence before the sample. The infrared and visible beams were focused on the samples by lenses with a focal length of 10 and 25 cm, had an incident angle of 53.5 ± 1° and 66 ± 1°, and had a size at the sample of 60 and 150 μm, respectively. After the sample the VSF signal was collimated by a lens (f = 350 mm) and focused again on the entrance slit of a spectrograph (Jobin Yvon, Triax 320). Finally, the dispersed signals were imaged on an iCCD camera (Princeton Instruments). The frequency of the resulting spectrum was calibrated with emission lines from a neon lamp and adsorption peaks from a polystyrene thin film when the nonresonant signal from the z-cut quartz was measured. After the SF polarizer a $\lambda/2$ plate was used to rotate the SF field such that the same polarization always propagated through the bulk of the detection path and into the camera. Between the sample and this $\lambda/2$ plate were two gold mirrors and a polarizer. The transmission/reflection efficiency of each of these three optical elements was shown to be polarization insensitive.

To account for the frequency-dependent IR pulse energy, we normalized the measured VSF response from the air/D_2O interface by the, nonresonant, VSF signal from z-cut quartz. Quartz lacks inversion symmetry and is thus bulk sum-frequency active. For this normalization measurement the quartz crystal was oriented such that the $x-z$ plane of the bulk unit cell is the beam incident plane: the quartz crystal is rotated to produce a maximum VSF signal. The acquisition time for measurements of the VSF spectral response of the z-cut quartz and D_2O were 30 and 300 s, respectively.

VSF spectra of three polarization combinations, namely *ssp* (*s*-polarized SF, *s*-polarized visible, and *p*-polarized IR), *sps* and *ppp* were measured for both D_2O and z-cut quartz. D_2O measurements were conducted using a homemade Teflon trough. Before measurement the trough was cleaned with ethanol in an ultrasonic bath for 30 min and then in Milli-Q water 5+ times before being dried with N_2. D_2O (Sigma-Aldrich) was used without further purification. Spectra of the visible beam as a function of pulse duration were measured by a fiber spectrometer (Ocean Optics), from which the Fourier-transform limited pulse durations were calculated. To check the accuracy of this transform limited pulse length, a cross-correlation between the spectrally narrowed visible beam and the broadband IR beam from a z-cut quartz was also measured. The two values were in quantitative agreement.

Analysis of the measured sum frequency spectral response was performed following previous studies.[12] In brief, the background signal (IR beam blocked) was first subtracted from the raw data for all spectra. The background-free D_2O spectrum was then divided by the background-free z-cut spectrum for the corresponding polarization combinations to account for the lineshapes of the IR light and the spatial overlap of the visible and infrared beams. The normalized spectra were then multiplied by the calculated second order susceptibility strength

(accounting for the Fresnel factors, the coherence length of the fields in quartz, and different camera parameters between sample and reference) of the z-cut quartz to obtain the absolute intensity of the effective susceptibilities of the D_2O. Because the second order nonlinear susceptibility of bulk quartz has been previously measured,[43] this procedure allows us, as done by prior authors, to report the measured squared modulus of the second order nonlinear susceptibility of the air/D_2O interface in atomic units ($m^4\ V^{-2}$).

Modeling of the spectral response was carried out by fitting a line shape model (discussed in detail below) to the corrected $|\chi^{(2)}_{eff}|^2$ using the Levenberg–Marquardt algorithm as implemented in the commercial visualization and analysis program Igor Pro (Wavemetrics). Sensitivity of the minimization to values of the initial guesses of each parameter was tested empirically (by varying initial guesses over several orders of magnitude). The reported uncertainty for each parameter extracted from the fit is the result of a linearization of the model, with respect to its parameters, after optimization of the model/data fit.

COMPUTATIONAL DETAILS

We performed all-atom molecular dynamics simulations of D_2O slabs using the molecular dynamics package NAMD.[44] The resulting trajectories were visualized and analyzed using the package VMD—Visual Molecular Dynamics.[45] We employed both the rigid, nonpolarizable water model SPC/E[46] and the rigid, polarizable model SWM4-NDP.[47] Following prior authors,[48,49] we form D_2O in both cases by replacing the isotopically weighted average hydrogen mass by the deuterium mass. The SPC/E model was selected for this study because it shows the best agreement with experiment of the most widely used nonpolarizable water models.[50] The SWM4-NDP model is based on classical Drude oscillators and was selected because it reproduces the vaporization enthalpy, density, static dielectric constant, and self-diffusion constant of water in the bulk, as well as the surface tension of the air–water interface. Comparison of the results from both water models allows us to conclude, as described in the following sections, that the observed qualitative trends are model-independent.

The initial configuration of the water slab, shown in Figure 2, contains 826 water molecules, is 3 × 3 × 3 nm^3, and was created using the equilibrated water box plugin available in VMD and VMD-based scripts. Electrostatic forces were calculated directly up to 15 Å and using the Particle Mesh Ewald method with 1 Å grid-spacing for larger distances. The van der Waals (VdW) energy was switched to zero between 13 and 15 Å, and long-range corrections to the energy or pressure were not used. The relatively large cut off for VdW interactions is necessary to improve agreement of interfacial properties, such as the surface tension, with experiment.[51−53] Prior work has indicated that long VdW cut offs are important even when interactions are dominated by the electrostatic component,[54,55] as is the case here. For the SPC/E model, the equations of motion were integrated using a modified Verlet algorithm with multiple time stepping, with electrostatic forces calculated every 2 fs and the remaining forces every 1 fs. For the SWM4-NDP model, integration was performed using an extended Lagrangian scheme with dual Langevin thermostats, with electrostatic interactions calculated every 1 fs and all other interactions calculated every 0.5 fs. This scheme, described in detail previously,[56] produces classical trajectories near the self-consistent field limit at a much lower computational cost than

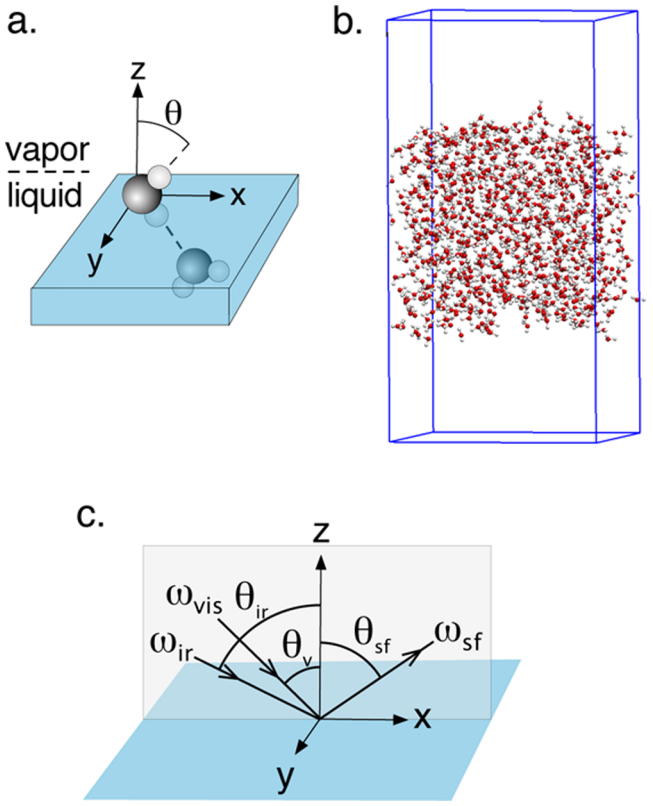

Figure 2. (a) External coordinate system used in the evaluation of experiment and simulation: the x–y plane is taken to be the plane of the surface and z is the surface normal. Angular heterogeneity is defined with respect to the angle (θ) between the free OD and the surface normal z. (b) 3 × 3 × 6 nm^3 simulation box. z = 0 is taken to be the time- and space-averaged position of the center-of-mass of the D_2O layer. (c) Experimental geometry indicating the incident and emitted beams, plane of incidence, and angles of all beams.

that involved in the actual self-consistent field procedure. The SETTLE algorithm was used to fix all bond lengths. A periodic simulation box with dimensions 3 × 3 × 6 nm^3 was used to minimize unphysical electrostatic interactions in the z direction, that is, the surface normal. Both systems were equilibrated for 1 ns in the canonical ensemble at 300 K to produce a stable water slab. Production runs for each water model were 0.8 ns long with configurations saved every 10 fs. To avoid the influence of the thermostat and barostat on dynamic properties, the production run for the SPC/E water model was performed in the microcanonical ensemble. As simulations of the SWM4-NDP model in that ensemble are computationally costly the production run for this model was instead performed in the canonical ensemble, but with the use of weak friction coefficients for the Langevin thermostats associated with the Drude particles (friction coefficient of 0.1 ps^{-1}) and the remaining degrees of freedom (0.05 ps^{-1}). Prior work has shown that such small friction coefficients significantly improve computational performance without measurably affecting the dynamical properties of the system.[56] The average temperatures during the production runs were $T_{SPC/E}$ = 299 ± 5 K and $T_{SWM4-NDP}$ = 300 ± 6 K. The total energy drift of the microcanonical production run was less than 1.5 × 10^{-3}%.

To calculate the properties of the free OD at the air/D_2O interface we require a means of defining the interface and of defining a hydrogen bond. Here we follow our prior work in

defining the interface, that is, a decrease of the time- and space-averaged density of free OD groups of 10% relative to bulk (see Supporting Information), and define a hydrogen bond as occurring, unless otherwise indicated, for O···O distances less than 3.5 Å and OD···O angles greater than 140°. We have previously shown that these criteria result in good agreement between structural and dynamic properties of interfacial water from simulation and from VSF experiments.[34,35] For consistency with experiment, some observables are calculated for interfacial OD groups that remain free for at least 60 fs; the population of OD used in the calculation of each observable is clearly indicated in the text. The effect of quantitatively different definitions of the interface or of hydrogen bonds on our conclusions is minimal and discussed in the Supporting Information. Unless otherwise indicated, the statistical uncertainty of reported computationally derived quantities is given as the standard deviation estimated using block averages.[57,58]

THEORETICAL DESCRIPTION OF VSF

Macroscopic Response. In this study we wish to determine whether the orientational distribution of the free OD changes with respect to the laboratory frame on the time scales of vibrational dephasing. We do this by measuring the polarization dependent sum frequency spectral response as a function of visible pulse length. To understand the connection of these experimental observables to molecular orientational distribution it is necessary to review the theoretical description of the sum frequency spectral response. For a VSF experiment employing a spectrally broad infrared pulse and spectrally narrow visible pulse in reflection geometry (see Figure 2c) the sum frequency intensity can be written:[12,36,59]

$$I_{sf} = \frac{8\pi^3 \omega_{SF}^2 \sec^2 \alpha_{sf}}{c^3 n_{air}(\omega_{sf}) n_{air}(\omega_{ir}) n_{air}(\omega_{vis})} \times |E_{vis} \otimes \chi_{eff}^{(2)}|^2 I_{ir} \quad (1)$$

in which ω_{sf}, ω_{vis}, and ω_{ir} are the frequencies of the sum frequency, visible, and infrared fields, $n_{air}(\omega_i)$ is the refractive index of air at frequency i, α_j is the incident angle of the beam j, I_{ir} is the infrared intensity (which is a function of frequency), E_{vis} is the visible field (also a function of frequency), $\otimes$ indicates a frequency domain convolution, and $\chi_{eff}^{(2)}$ is the effective second-order susceptibility of the interface. $\chi^{(2)}$ is a third rank tensor. Of its 27 terms, 7 are nonzero at an interface, such as the air/water, with rotational symmetry around the surface normal (macroscopic $C_{\infty v}$ symmetry).[12,60]

Given an external coordinate system (see Figure 2a,c) in which the air/water interface is the $x-y$ plane, all beams propagate in the $x-z$ plane, and an $s(p)$ polarized beam indicates a field vector in the $x-y(x-z)$ plane, measuring the free OD VSF spectral response at three independent polarization combinations will sample six of these seven terms in the following manner:[12,59,61]

$$\begin{aligned}
\chi_{eff,ssp}^{(2)} &= L_{yy,\omega_{sf}} L_{yy,\omega_{vis}} L_{zz,\omega_{ir}} \sin \alpha_{ir} \chi_{yyz}^{(2)} \\
\chi_{eff,sps}^{(2)} &= L_{yy,\omega_{sf}} L_{zz,\omega_{vis}} L_{yy,\omega_{ir}} \sin \alpha_{vis} \chi_{yzy}^{(2)} \\
\chi_{eff,ppp}^{(2)} &= -L_{xx,\omega_{sf}} L_{xx,\omega_{vis}} L_{zz,\omega_{ir}} \cos \alpha_{sf} \cos \alpha_{vis} \sin \alpha_{ir} \chi_{xxz}^{(2)} \\
&\quad - L_{xx,\omega_{sf}} L_{zz,\omega_{vis}} L_{xx,\omega_{ir}} \cos \alpha_{sf} \sin \alpha_{vis} \cos \alpha_{ir} \chi_{xzx}^{(2)} \\
&\quad + L_{zz,\omega_{sf}} L_{xx,\omega_{vis}} L_{xx,\omega_{ir}} \sin \alpha_{sf} \cos \alpha_{vis} \cos \alpha_{ir} \chi_{zxx}^{(2)} \\
&\quad + L_{zz,\omega_{sf}} L_{zz,\omega_{vis}} L_{zz,\omega_{ir}} \sin \alpha_{sf} \sin \alpha_{vis} \sin \alpha_{ir} \chi_{zzz}^{(2)}
\end{aligned} \quad (2)$$

Following common practice, polarization combinations are referred in the order *sf*, *vis*, *ir*. Thus the term $\chi_{eff,ssp}^{(2)}$ indicates the $\chi_{eff}^{(2)}$ as measured with an *s* polarized sum frequency, *s* polarized visible, and *p* polarized infrared beam. The Fresnel coefficients, the L_{ii} terms, project the far-field sum frequency, visible, and infrared fields onto the interface and are a function of the refractive index of bulk water (trivially of bulk air) and the interface at the relevant frequencies as well as the incident and reflected angles of the beams. These coefficients have been tabulated previously[12,61] and are reproduced in the Supporting Information for completeness.

Connecting the Macroscopic and Molecular Response. If interfacial molecules have an orientational distribution and rotate slowly with respect to the time scale set by the resonance line width (T_2), the macroscopic susceptibility can be linked to the microscopic hyperpolarizability tensor ($\beta_{i'j'k'}^{(2)}$ given in the molecular coordinate frame (i', j', k')),[7,62]

$$\chi_{ijk}^{(2)} = N \sum_{i'j'k'} \langle R_{ii'} R_{jj'} R_{kk'} \rangle \beta_{i'j'k'}^{(2)} \quad (3)$$

where $R_{aa'}$ is the matrix element of the Euler transformation matrix from the molecular coordinates (i' j' k') to the laboratory coordinate (ijk), N is the molecular number density and the $\langle\rangle$ indicate an ensemble average over an appropriate orientational distribution (discussed in detail below). It is as a consequence of the relationship between $\chi^{(2)}$ and $\beta^{(2)}$ encoded in eq 3 that molecular orientation information can be inferred from measuring different components of $\chi_{ijk}^{(2)}$. The molecular hyperpolarizability contains both a resonant (frequency dependent) and nonresonant component. If the resonant response is homogeneously broadened (the applicability of this assumption to the free OD is discussed below) it can be modeled as a sum of Lorentzians,

$$\beta_{i'j'k'}^{(2)} = \beta_{nr,i'j'k'}^{(2)} + \sum_n \frac{\beta_{n,i'j'k'}}{\omega_{ir} - \omega_n + i\Gamma_n} \quad (4)$$

in which ω_{ir} is the infrared frequency, $\beta_{nr,i'j'k'}^{(2)}$ is the nonresonant complex amplitude, $\beta_{n,i'j'k'}$ is the complex amplitude of resonance n, and ω_n is the center frequency and Γ_n is the damping constant of resonance n. For data analysis eq 4 is typically substituted into eq 3 giving,

$$\chi_{ijk}^{(2)} = |\chi_{nr}| e^{i\varepsilon} + \sum_n \frac{\chi_{n,ijk}}{\omega_{ir} - \omega_n + i\Gamma_n} \quad (5)$$

in which ε is the relative phase of the nonresonant background (and is here taken to be independent of ω), χ_{nr} is the nonresonant, and χ_n is the resonant amplitude.

dx.doi.org/10.1021/jp406577v | J. Phys. Chem. B 2013, 117, 11753−11764

The damping constant of the nth Lorentzian (Γ_n) contains a contribution due to pure dephasing (with characteristic time T_2^*) and lifetime (with characteristic time T_1),

$$2\pi c\Gamma_n = \frac{1}{T_{2,n}} = \frac{1}{T_{2,n}^*} + \frac{1}{2T_{1,n}} \quad (6)$$

in which c is the speed of light.

As is clear from eq 1, in a broadband VSF measurement the observed signal is a convolution of the frequency-dependent visible field and the frequency dependent material response $\chi_{\text{eff}}^{(2)}$. For an infinitely spectrally narrow visible pulse, the peaks apparent in the measured I_{sf} spectra are, thus, to within the resolution of the spectrometer, the resonant material response. For visible pulses of finite spectral width some broadening of the observed resonance must occur.

One way to understand the origin of this broadening is to consider the Fourier transformed susceptibility: the susceptibility in the time domain. In this picture (shown in cartoon form in Figure 3) it becomes clear that the visible pulse is a window function of the resonant polarization induced by the infrared field (see discussion by Stiopkin and co-workers and Laaser and co-workers[36,63]). As the visible field becomes spectrally broader it is temporally shorter: up conversion of long time behavior of the induced polarization (equivalently the wings of the peak in the frequency domain) is inefficient. This broadening is thus not related to the material being probed and is well understood in the VSF spectroscopy community: it can be straightforwardly accounted for by separately measuring the spectrum of the visible pulse and then deconvoluting the frequency dependent visible field (E_{vis}) from the I_{sf} before analysis.[36]

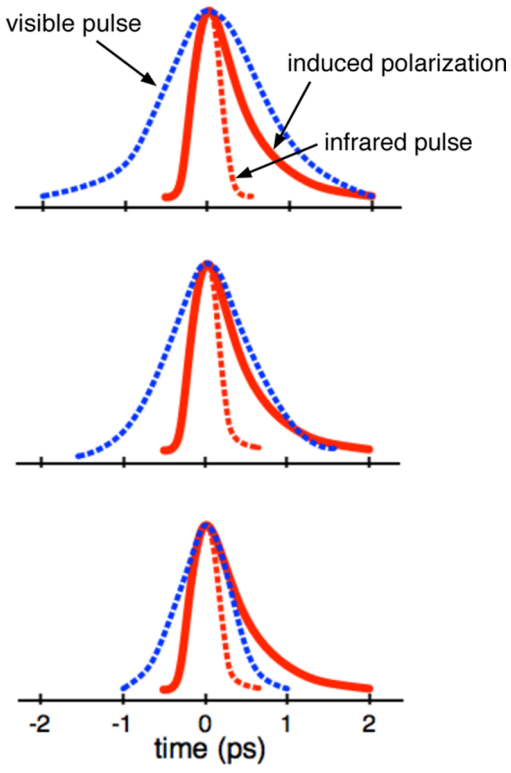

Figure 3. Cartoon indicating the premise of the experiment. The dashed red line is the infrared pulse, the solid red line is the induced polarization (the free induction decay (FID)), and the dashed blue line is the visible pulse. Clearly as the visible pulse length is shortened, earlier portions of the FID are preferentially sampled.

Experimental Concept. Given a single homogeneously broadened resonance in the frequency domain, that is, a Lorentzian, the resulting time domain signal decays exponentially. Such a response suggests material properties do not change as a function of visible pulse length: the properties of this exponentially decaying signal do not depend on where we sample it and do not depend on the length of the visible pulse (i.e., the window function) used to up convert the signal. If, on the other hand, the orientational distribution underlying this emission changes on the time scale of dephasing (T_2) this condition is no longer met. Because the ratio of VSF spectral intensities measured with different polarizations is a function of molecular orientation (see eq 3) this sort of structural dynamical heterogeneity should be apparent in these intensity ratios changing with visible pulse length.

As discussed in the introduction, simulation and prior experiment suggest that the free OD vibrational lifetime is at least partly due to rotation of the free OD toward bulk and the formation of a hydrogen bond and that this structural relaxation channel is heterogeneous: free OD groups on water molecules closer to vapor tend to be differently oriented and to live longer before rotating down and forming a hydrogen bond, than those closer to bulk liquid. In what follows, we experimentally test this proposition by measuring the polarization-dependent sum frequency emission of the free OD of D_2O as a function of visible pulse length. We then compare it to the free OD orientational distributions simulated with a similar window function.

EXPERIMENTAL AND COMPUTATIONAL RESULTS

Free OD Heterogeneity in Simulation. As discussed above, we have previously shown in classical all atom molecular dynamic simulations of the air/H_2O interface employing both the SPC/E and TIP4P/2005 potentials that, as one moves from bulk liquid H_2O toward vapor, the orientational distribution of the free OH narrows and points closer to the surface normal and the characteristic time scale before rotation toward the liquid and formation of a hydrogen bond grows longer (see Figure 1).[34,35] Here we performed a similar analysis for the air/D_2O interface employing both the SPC/E fixed charge and the SWM4-NDP polarizable water models using longer production trajectories than in our previous work. We investigate the connection between the lifetime of free OD groups and their average orientation at the surface by calculating the fraction, $f(\theta, t)$, of interfacial OD groups that remains continuously free for time t, and that forms angle θ with the surface normal at time t (see Figure 2a for the coordinate system used here):

$$f(\theta, t) = \frac{\langle n_{[0,t]}(\theta_t)\rangle}{\langle n_{t=0}\rangle} \quad (7)$$

In this expression, $n_{[0,t]}(\theta_t)$ is the number of interfacial OD groups that remain continuously free within the interval $[0,t]$ and that at time t form angle θ with the surface normal. $n_{t=0}$ is then the total number of free, interfacial, OD groups at $t = 0$. For both quantities the angled brackets indicate averaging over all time origins. For both D_2O models, OD groups are considered interfacial if their oxygen atom has $|z| > 10$ Å, that is, it belongs to the outer regions of the water slab (see Supporting Information for details). The connection between the interfacial z position and the orientation of interfacial OD

dx.doi.org/10.1021/jp406577v | J. Phys. Chem. B 2013, 117, 11753−11764

groups is investigated by calculating the fraction $f(\theta, z)$ of OD groups at each position z that forms an angle θ with the surface normal, according to

$$f(\theta, z) = \frac{\langle n(\theta, z)\rangle}{\langle n(z)\rangle} \quad (8)$$

Here $\langle n(\theta,z)\rangle$ is the time averaged number of free OD groups at each position z that form angle θ with the surface normal. We use $\langle n(z)\rangle$, the time averaged total number of free OD groups at the same position, as the normalization constant so that $f(\theta, z)$ conveys the preferential orientation of OD groups *at each* z: for each z, $f(\theta,z) = 0$ if no OD groups have orientation θ and $f(\theta, z) = 1$ if all OH groups at that z position point in that direction. The quantities $f(\theta, t)$ and $f(\theta, z)$ are shown in Figure 4 for the SPC/E model, and in the Supporting Information for the SWM4-NDP model. As is clear from inspection, both water models show similar trends to that previously observed for the air/H_2O interface. First, as one moves from (bulk) liquid water toward air (along the z-coordinate in Figure 2a) the average angle of the free OD with respect to the surface normal decreases and the distribution narrows. Second, free ODs with a longer τ_{reor}—free ODs that live longer before rotating toward the bulk to form a hydrogen bond—have an average orientation closer to the surface normal and a narrower orientational distribution than those characterized by smaller values of τ_{reor}.

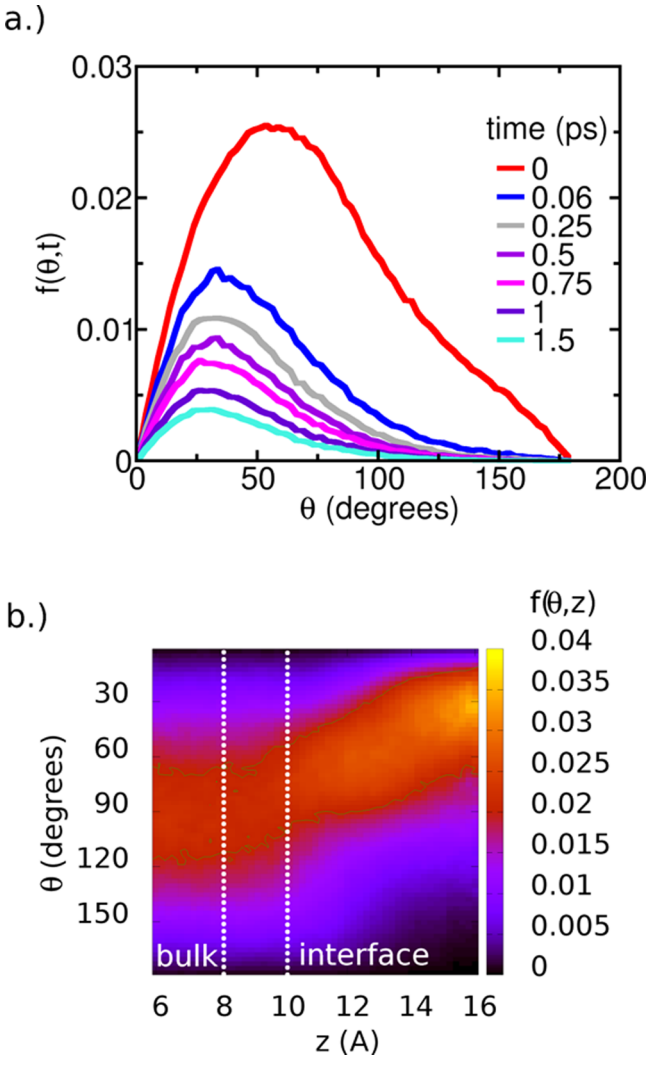

Figure 4. (a) Orientational distribution, $f(\theta,t)$, of SPC/E free OD groups at the air/D_2O interface as a function of sampling window: for example, the blue line indicates the orientational distribution of all free ODs that have not rotated toward liquid and formed a hydrogen bond within 60 fs or, equivalently, all free OD whose $\tau_{reor} > 60$ fs. As indicated other lines show similar populations at longer times. (b) The orientational distribution, $f(\theta, z)$, of SPC/E free ODs as a function of position within the simulated water slab ($z < 8.0$ Å is in bulk D_2O, $z >$ 10 Å is vapor). Similar qualitative trends are found using SWM4-NDP D_2O (see Supporting Information).

VSF Free OD Spectral Response. As discussed above we wish to determine whether the structural heterogeneity apparent in simulation can also be observed in measurement of the free OD $I_{sf,ppp}$, $I_{sf,sps}$ and $I_{sf,ssp}$ spectral response(s) as a function of visible pulse length. In Figure 5 the measured $I_{sf,ppp}$ and $I_{sf,ssp}$ data are shown after correction for Fresnel factors, frequency-dependent infrared energy and quartz coherence length. Similarly corrected $I_{sf,sps}$ data are shown in the Supporting Information. Consistent with prior measurements, the apparent resonance intensity under the *sps* polarization condition is much lower than that measured under both *ppp* and *ssp* and is thus not here discussed further.[7,12] Four qualitative conclusions can be made from inspection of Figure 5. First, consistent with prior results both using H_2O and D_2O,[6,12,64] we see two resonances (regardless of visible pulse length): a narrow peak centered at ~2735 cm^{-1} and a wider peak centered at frequencies below our spectral window (this peak is particularly apparent in the *ppp* spectrum through its interference with the free OD). Following much prior work, we assign the narrow peak to the free OD and the broader, lower frequency peak to the high frequency tail of the hydrogen-bonded OD response. Second, as expected from the free OD orientation and our experimental geometry, $|\chi^{(2)}_{eff,ppp}|^2 > |\chi^{(2)}_{eff,ssp}|^2$ ($>|\chi^{(2)}_{eff,sps}|^2$ (see Supporting Information)). Third, as the visible

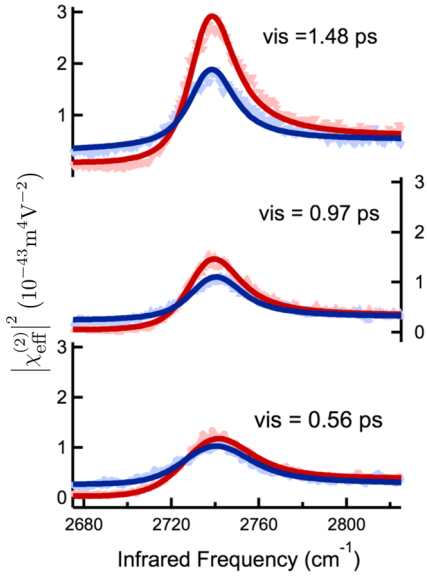

Figure 5. $|\chi^{(2)}_{eff,ppp}|^2$ (red) and $|\chi^{(2)}_{eff,ssp}|^2$ (blue) corrected for the Fresnel factors, frequency-dependent infrared power and quartz coherence length, of the free OD as a function of visible pulse length. Points are data, solid lines are fits to the data using the line shape model discussed in the text. Clearly the $((|\chi^{(2)}_{eff,ppp}|^2)/(|\chi^{(2)}_{eff,ssp}|^2))$ ratio changes as a function of visible pulse length.

dx.doi.org/10.1021/jp406577v | J. Phys. Chem. B 2013, 117, 11753−11764

Table 1. Results from Fitting the Line Shape Model in eq 5 Using the Strategy Described in the Text and Supporting Information

	ppp	*ssp*	*ppp*	*ssp*	*ppp*	*ssp*
vis pulse length (ps)	1.48		0.97		0.56	
$\Delta\omega_{vis}$ (cm^{-1})	9.9		14.6		24.0	
χ_{nr}	0.85 ± 0.01	0.74 ± 0.01	0.63 ± 0.01	0.55 ± 0.01	0.72 ± 0.01	0.50 ± 0.01
ε	2.4 ± 0.04	1.9 ± 0.04	2.4	1.9	2.4	1.9
χ_{free}	**14.1 ± 0.2**	**8.2 ± 0.1**	**10.8 ± 0.2**	**6.7 ± 0.1**	**11.2 ± 0.3**	**7.85 ± 0.2**
ω_{free} (cm^{-1})	2735 ± 0.2	2736 ± 0.4	2735 ± 0.2	2738 ± 0.2	2735 ± 0.3	2737 ± 0.5
Γ_{free} (cm^{-1})	10		10		10	
χ_{D-b}	−39.0 ± 1.7	−13.0 ± 1.6	−28.4 ± 1.0	−4.0 ± 0.9	−40.9 ± 1.1	2.3 ± 1.4
ω_{D-b} (cm^{-1})	2633		2633		2633	
Γ_{D-b} (cm^{-1})	80		80		80	

pulse gets spectrally broader (temporally shorter) the measured line width of the free OD appears to increase (as expected from eq 1). Finally, and most importantly, the measured $((|\chi^{(2)}_{eff,ppp}|^2)/(|\chi^{(2)}_{eff,ssp}|^2))$ ratios change as a function of the temporal length of the visible pulse used to make the measurement. The observation that the ratios of polarization-dependent free OD sum frequency response change as a function of sampling window is consistent with a scenario in which free OD interfacial structure is lifetime dependent. As is clear in simulation and has been suggested by previous IR pump/VSF probe measurements,[34,35] evidently the interfacial free OD is structurally heterogeneous on the time scale of vibrational dephasing (T_2).

Extracting Orientational Information from the VSF Spectral Response. To quantify this heterogeneity we first need to quantify the macroscopic resonant response of the free OD as a function of visible pulse length and then connect this macroscopic response to molecular level orientation. As discussed above, assuming the reorientation rate of the free OD is slow relative to vibrational dephasing, existing theory allows the accomplishment of both steps. Following prior workers we initially fit the data using the line shape model described in eq 5. As discussed in detail in the Supporting Information, this line shape model overparameterizes the data: multiple descriptions of the data are possible for different values of each parameter. To overcome this problem we assume the following: (1) The hydrogen-bonded OD center frequency is, as discussed in detail previously, the mass scaled center frequency of the hydrogen bonded OH center frequency.[12,15] (2) The line widths of the hydrogen bonded (Γ_{D-B}) and free OD (Γ_{free}) do not depend on beam polarizations. (3) The nonresonant phase does not change as a function of visible pulse length (it always temporally overlapped with the much shorter infrared pulse). The results of this approach are shown (for the *ssp* and *ppp* data) in Table 1 (see the Supporting Information for more detailed discussion). We note here in passing, that the line width of the free OD (Γ_{free}) was allowed to vary in this fit description: apparently any variation in Γ_{free} as a function of visible pulse length is, after accounting for visible pulse spectrum, too small to resolve in our measurements.

After extracting the χ_{free} for each polarization condition and visible pulse length we can in principle, using the line shape model discussed above, directly calculate molecular orientation from a single observation. In practice doing so is extremely challenging. Here then we follow much prior work and infer orientation from the ***ratio*** of measured quantities.[7,12,61] This approach means that, for a particular visible pulse length, we have one independent constraint on free OD orientation, $((\chi_{free,ppp})/(\chi_{free,ssp}))$, and thus can quantify only the first moment of an arbitrary free OD orientational distribution. The lack of insight into the type of orientational distribution characteristic of a particular surface-bound moiety is a general problem in VSF orientational analysis and has been previously dealt with, in a variety of systems, by assuming either a delta function, in which case only one observable is required, or a Gaussian, in which case two observables are required and the distribution is assumed to be symmetric.[12,61]

Determining an Appropriate Orientational Distribution. Because the measurement furnishes no insight into the appropriate type of orientational distribution to analyze the VSF data we turn to our simulation results for this purpose. In principle the sort of histograms shown in Figure 4 furnish this insight. Here, however, to more closely approximate the measurement we calculate a histogram that includes all free OD groups present at the interface and, within a particular time window, weights the contribution of individual free ODs to the histogram by the time each has remained free. The latter qualification differs from the histograms shown in Figure 4a as there only populations of free OD groups that had remained free for ***at least*** the indicated period were included. The calculated function is

$$P_\tau(\theta) = \frac{\int_{\tau_0}^{\tau} n_{[0,t]}(\theta_t)\,dt}{\Delta\theta \int_{\tau_0}^{\tau} n_{[0,t]}\,dt} \tag{9}$$

where $n_{[0,t]}(\theta_t)$ is the number of interfacial OD groups that remain continuously free within $[0,t]$ and at time t form angle θ with the surface normal, $n_{[0,t]}$ is the total number of interfacial, OD groups that remain continuously free in the same time interval, and $\Delta\theta$ is the width of the histogram bin. A representative series of histograms calculated in this manner is shown in Figure 6. Clearly the orientational distribution is broad and asymmetric and the degree of this asymmetry changes as a function of sampling window although the changes are significantly smaller than those apparent in Figure 4 because of the lifetime weighted averaging. Because we adapt a geometric definition for hydrogen bonding in our simulation, in principle our results could be dominated by a subpopulation of free ODs that rapidly *flip* between a free and hydrogen bonded state. We tested sensitivity to this population by constructing similar orientational histograms of populations of free ODs that have existed for more than some threshold time τ_0. For all results shown τ_0 is taken to be 60 fs. Sensitivity tests with τ_0 = 0, 60, 100, 140 fs show our qualitative conclusions are

dx.doi.org/10.1021/jp406577v | J. Phys. Chem. B 2013, 117, 11753−11764

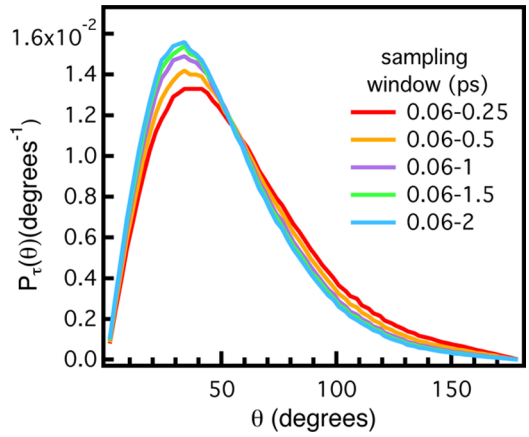

Figure 6. Lifetime weighted probability density, $P_\tau(\theta)$, of the free OD orientation as a function of the sampling window, [0.06, τ] ps, calculated for the SPC/E D_2O model.

insensitive to this choice, and they are discussed in more detail in the Supporting Information.

To choose an appropriate orientational distribution to describe our data, then, we require a function that is broad, asymmetric, and employs as few free parameters as possible (given our limited number of independent observations). Within these constraints we chose to employ a log-normal distribution. As discussed in more detail in the Supporting Information, it is clear that this choice is not unique—in general a log-normal distribution becomes a progressively better fit as one goes to longer sampling windows, and its goodness of fit depends on the water model. However, as long as the experiment and simulation sample similar underlying physics any errors introduced by this assumed orientational distribution should equally effect the mode (θ_0) and standard deviation (σ) inferred from both simulation and experiment.

Comparing Simulation and Experiment. Given a log-normal distribution and the hyperpolarizability ($\beta_{n,i',j',k'}$) from prior work[65] of the free OD, we solve the line shape model (eq 5, eq 3, and eq 1) and directly compare the experimentally derived orientation to those extracted from simulation. This comparison is shown for the orientation inferred from the $\chi_{free,ppp}/\chi_{free,ssp}$ ratio in Figure 7.

Two features of this comparison are immediately apparent. (1) The trend in the simulation is consistent with experiment: in general longer visible pulses sample populations of the free OD that have a smaller value of θ_0 and, possibly, a smaller value of σ than shorter visible pulses. (2) Regardless of experimental observable or water model, orientations inferred from simulation are systematically offset from those inferred from experiment (in the sense that experiments always suggest a smaller value of θ_0 and possibly a smaller value of σ than is apparent in the simulation).

A variety of factors may be responsible for the systematic offset between data and simulation. One possible explanation lies in the ensemble averaged transformation matrix in eq 3. As written, this matrix is expressed in the slow motion limit: the individual oscillators that contribute to the signal are assumed to be stationary on the time scale set by dephasing (T_2) and the observed orientational distribution is a function of quasi-static structural heterogeneity.[7,12,62] Prior experiment and simulation studies of the air/water interface, in part by us, suggest that this is likely a poor approximation.[34,35] Indeed in our simulations, as shown in Table 2, free OD groups experience a change in

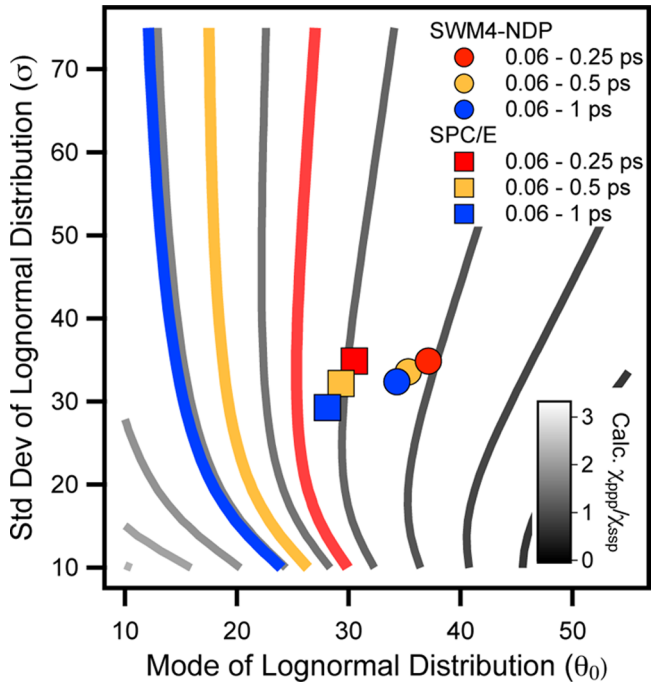

Figure 7. Calculated $\chi_{free,ppp}/\chi_{free,ssp}$ ratio as a function of mode and standard deviation of a log-normal distribution (black→gray lines). Measured $\chi_{free,ppp}/\chi_{free,ssp}$ ratios from experiment are 1.72 (visible pulse = 1.48 ps), 1.6 (visible pulse = 0.97 ps) and 1.42 (visible pulse = 0.56 ps). These values are consistent with the mode and standard deviations of a log-normal distribution indicated by the blue, orange, and red contours, respectively. Mode and standard deviation of log-normal distributions fitted to the simulation output for the two water models as a function of sampling window are shown as circles (SWM4-NDP) and squares (SPC/E) for comparison.

Table 2. Lifetime-Weighted Average Angular Displacement of Free, Interfacial, OD Groups as a Function of Sampling Window and Water Model

	angular displacement (deg)	
time (fs)	SPC/E	SWM4-NDP
60	19.2	21.0
100	22.9	25.5
250	24.2	28.1
500	26.7	30.3
750	27.1	30.6
1000	27.4	31.2

orientation on average of 19 − 30° during the vibrational dephasing (T_2) of the free OD (see Supporting Information for details of the calculation). Clearly the orientation of the free OD changes significantly on the time scale of vibrational dephasing. Shen and co-workers have pointed out that a similarly compact form of the transformation matrix is available under the assumption that individual free OD groups sample the entire orientational distribution during vibrational dephasing: the ***fast motion*** limit.[7,62] Comparison of Figure 6 and Table 2 clarifies that the average free OD angular displacement is less than the angular distribution width; that is, clearly individual ODs do not sample the entire distribution. As described by Shen and co-workers,[7,62] in this intermediate regime the form of the transformation matrix in eq 3 is time dependent and must be explicitly calculated. Such a calculation is beyond the current scope of this paper.

dx.doi.org/10.1021/jp406577v | J. Phys. Chem. B 2013, 117, 11753−11764

The shortcoming in our ability to interpret the free OD VSF response could be overcome if our visible pulses (sampling windows) were sufficiently short: if we performed a polarization resolved measurement of the free OD in the time domain. In such an experiment, each laser shot samples only a small portion of the temporal decay of the induced polarization and thus, on the time scale of the up conversion pulse, the motion of the free OD would be minimal and the slow motion limit appropriate. We are currently pursuing such measurements in our group.

While the incorrect description of free OD motion in relating the molecular and macroscopic length scales seems the most likely explanation for the disagreement between experiment and computation, other effects may also contribute. In analyzing our simulation results we have here assumed the vibrational lifetime is only a function of reorientation: free ODs are no longer counted as free when they rotate down and form a hydrogen bond. Clearly other vibrational relaxation mechanisms are possible. For example, prior work has suggested that vibrational relaxation of the free OD may occur through both rotation and intramolecular coupling (relaxation from the excited free OD to the hydrogen-bonded OD on the other half of the same molecule[66]). Adding this additional relaxation channel, with no further effects, would increase the disagreement between simulation and experiment: it is equivalent to preferentially sampling OD orientation at even earlier times (when values of σ and θ_0 are both larger).

It is, of course, possible that some additional vibrational relaxation channel may also exist for the free OD and that the efficiency of this pathway may change as a function of the free OD's position along the surface normal. Such a mechanism would be qualitatively consistent with the trend in our data if it acted to significantly decrease the lifetime of free OD groups that were close to bulk liquid relative to those closer to the vapor. In principle we should see such an effect in the line width (Γ_{free}), however, as illustrated in eq 6, observing such changes in our data is difficult for two reasons: our measurement scheme averages over all lifetimes within an expanding window function (Figure 3) and the factor of 2 in the denominator with T_1 in eq 6 minimizes the effect of lifetime on the measured line width relevant to that of pure dephasing (T_2^*). Because the time domain measurement described above would integrate over significantly smaller sampling windows, it would presumably be influenced to a larger degree by potential heterogeneity in the vibrational relaxation mechanism.

Finally, the systematic offset between simulation and experiment may be the result of a water model that is incorrect or a nonphysical definition of either the interface or a hydrogen bond. We tested this possibility by systematically fitting log-normal distributions to free OD ensembles generated with these changing boundary conditions. The result is shown in the Supporting Information. Clearly changing either water model, interface definition or hydrogen-bond definition leads to a quantitative change in the parameters describing the log-normal distribution fit to the simulation results; however, the systematic offset between model and data persists for all such combinations.

SUMMARY AND CONCLUSIONS

Simulation and prior IR pump/VSF probe experiments have suggested that the free OD of D_2O at the air/D_2O interface is structurally and dynamically heterogeneous: as one moves from the bulk liquid side of the interface toward vapor the free OD orientational distribution becomes narrower and the median of the distribution closer to the surface normal.[34,35] In this work we have shown that these trends persist both in longer simulations using the SPC/E, classical, fixed charge potential and in simulations using the classical polarizable SWM4-NDP potential.

If such heterogeneity occurs it should also be apparent in the free OD polarization-dependent sum frequency intensity as a function of the upconversion pulse duration. Here we show that measurements of the polarization-dependent free OD vibrational sum frequency spectral response are consistent with this inferred structural heterogeneity: the ratio of the amplitude of the free OD resonance sampled at different polarizations is clearly a function of visible pulse duration. To quantify this structural heterogeneity we employ existing VSF phenomenological theory. Interestingly we find a systematic offset between free OD orientation (with changing visible pulse length) as inferred from the measured $\chi_{free,ppp}/\chi_{free,ssp}$ ratio and simulation. This offset is most simply understood as a challenge in relating the macroscopic susceptibility to the molecular hyperpolarizability for the free OD. Simulation strongly suggests that the free OD is intermediate between the fast motion and slow limits and thus, for quantitative description of the microscopic origin of measured trends, a time-dependent, ensemble-averaged transformation matrix between the two coordinate systems is required. Such theory is beyond the scope of this study.

The consistency of our new experimental and simulation results offers further evidence of the free OH interfacial structural heterogeneity at the air/water interface. This heterogeneity has several interesting implications. Prior simulation and VSF studies have found that various salts are surface active at the air/water interface to varying degrees.[1,67] In some cases this surface activity results in a decrease in intensity of the observed free OH response.[13] This decrease in intensity has been interpreted as indicating a decrease in free OH population: free OH groups rotate toward the bulk and donate a hydrogen bond (either to an anion or bulk water). Our results suggest that if surface active anions are sequestered at the air/water interface but relatively close to bulk it should be possible to see a decrease in free OH structural heterogeneity in the presence of these anions. The contribution of the relatively short-lived population of free ODs close to the bulk liquid whose orientation is on average both relatively far from the surface normal and relatively broad to the measured signal would be suppressed.

Both our experimental VSF results and the simulation average over small scale structural inhomogeneity. This averaging leads to *smoothed* density profiles in simulation at the air/water interface and has been shown to be the result of capillary waves.[68,69] Much as this averaging acts to smooth local density profiles, it should also act to smooth differences in free OH orientational distribution. It therefore seems likely that the effect we observe should be even more apparent where water meets hydrophobic solid or liquid phases at which such fluctuations are expected to be suppressed.

Finally we note that our results clarify that a measurement of $|\chi_{eff}^{(2)}|^2$ samples different populations as a function of the length of the visible (i.e., upconversion) pulse. Several previous studies have explored the possibility of enhancing spectral resolution in a frequency domain VSF measurement of $|\chi_{eff}^{(2)}|^2$ by delaying the visible relative to the IR pulse.[36−38] This approach is attractive because it both potentially reduces the nonresonant contribu-

tion to the measured $|\chi^{(2)}_{eff}|^2$ and, for certain visible pulse shapes, increases spectral resolution. Our work clarifies that for the free OD such a scheme would also sample different water subpopulations. Because the physics underlying this effect at the air/water interface are general, such enhancement schemes should only be used with caution.

■ ASSOCIATED CONTENT

Supporting Information

Detailed description of line shape analysis, discussion of the *sps* data, evaluation of sensitivity of the simulation results to hydrogen bond and interface definition, angular displacement comparison of D_2O and H_2O and interfacial orientation and lifetime at the air/D_2O interface using the SWM-NDP4 model. This material is available free of charge via the Internet at http://pubs.acs.org.

■ AUTHOR INFORMATION

Corresponding Author

*E-mail: campen@fhi-berlin.mpg.de. Tel.: +49 30 8413-5230. Fax: +49 30 8413-5106.

Notes

The authors declare no competing financial interest.

■ ACKNOWLEDGMENTS

The authors thank Tobias Kampfrath for his careful reading of the manuscript and Harald Kirsch for his help in conducting the measurements. Y.T. and R.K.C. acknowledge the continued financial support of the Physical Chemistry Department (and its director Martin Wolf) of the Fritz Haber Institute of the Max Planck Society. A.V.V. acknowledges similar support from the Department of Theory and Biosystems (and its director Reinhard Lipowsky) of the Max Planck Institute of Colloids and Interfaces.

■ REFERENCES

(1) Jungwirth, P.; Tobias, D. J. Specific Ion Effects at the Air/Water Interface. *Chem. Rev.* **2006**, *106*, 1259−1281.
(2) Dash, J. G.; Rempel, A. W.; Wettlaufer, J. S. The Physics of Premelted Ice and Its Geophysical Consequences. *Rev. Mod. Phys.* **2006**, *78*, 695−741.
(3) Chandler, D. Interfaces and the Driving Force of Hydrophobic Assembly. *Nature* **2005**, *437*, 640−647.
(4) Steiner, T. The Hydrogen Bond in the Solid State. *Angew. Chem., Int. Ed.* **2002**, *41*, 48−76.
(5) Zhu, X. D.; Suhr, H.; Shen, Y. R. Surface Vibrational Spectroscopy by Infrared-Visible Sum Frequency Generation. *Phys. Rev. B* **1987**, *35*, 3047−3050.
(6) Du, Q.; Superfine, R.; Freysz, E.; Shen, Y. R. Vibrational Spectroscopy of Water at the Vapor Water Interface. *Phys. Rev. Lett.* **1993**, *70*, 2313−2316.
(7) Wei, X.; Shen, Y. R. Motional Effect in Surface Sum-Frequency Vibrational Spectroscopy. *Phys. Rev. Lett.* **2001**, *86*, 4799−4802.
(8) Richmond, G. L. Structure and Bonding of Molecules at Aqueous Surfaces. *Annu. Rev. Phys. Chem.* **2001**, *52*, 357−389.
(9) Richmond, G. L. Molecular Bonding and Interactions at Aqueous Surfaces as Probed by Vibrational Sum Frequency Spectroscopy. *Chem. Rev.* **2002**, *102*, 2693−2724.
(10) Shultz, M.; Baldelli, S.; Schnitzer, C.; Simonelli, D. Aqueous Solution/Air Interfaces Probed with Sum Frequency Generation Spectroscopy. *J. Phys. Chem. B* **2002**, *106*, 5313−5324.
(11) Raymond, E. A.; Tarbuck, T. L.; Brown, M. G.; Richmond, G. L. Hydrogen-Bonding Interactions at the Vapor/Water Interface Investigated by Vibrational Sum-Frequency Spectroscopy of HOD/H_2O/D_2O Mixtures and Molecular Dynamics Simulations. *J. Phys. Chem. B* **2003**, *107*, 546−556.
(12) Gan, W.; Wu, D.; Zhang, Z.; Feng, R. R.; Wang, H.-F. Polarization and Experimental Configuration Analyses of Sum Frequency Generation Vibrational Spectra, Structure, and Orientational Motion of the Air/Water Interface. *J. Chem. Phys.* **2006**, *124*, 114705.
(13) Gopalakrishnan, S.; Liu, D. F.; Allen, H. C.; Kuo, M.; Shultz, M. J. Vibrational Spectroscopic Studies of Aqueous Interfaces: Salts, Acids, Bases, and Nanodrops. *Chem. Rev.* **2006**, *106*, 1155−1175.
(14) Levering, L. M.; Sierra-Hernandez, M. R.; Allen, H. C. Observation of Hydronium Ions at the Air−Aqueous Acid Interface: Vibrational Spectroscopic Studies of Aqueous HCl, HBr, and HI. *J. Phys. Chem. C* **2007**, *111*, 8814−8826.
(15) Sovago, M.; Campen, R. K.; Bakker, H. J.; Bonn, M. Hydrogen Bonding Strength of Interfacial Water Determined with Surface Sum-Frequency Generation. *Chem. Phys. Lett.* **2009**, *470*, 7−12.
(16) Fan, Y.; Chen, X.; Yang, L.; Cremer, P. S.; Gao, Y. Q. On the Structure of Water at the Aqueous/Air Interface. *J. Phys. Chem. B* **2009**, *113*, 11672−11679.
(17) Jubb, A. M.; Hua, W.; Allen, H. C. Environmental Chemistry at Vapor/Water Interfaces: Insights from Vibrational Sum Frequency Generation Spectroscopy. *Annu. Rev. Phys. Chem.* **2012**, *63*, 107−130.
(18) Sovago, M.; Campen, R. K.; Wurpel, G. W. H.; Müller, M.; Bakker, H. J.; Bonn, M. Vibrational Response of Hydrogen-Bonded Interfacial Water Is Dominated by Intramolecular Coupling. *Phys. Rev. Lett.* **2008**, *100*, 173901.
(19) Sovago, M.; Campen, R. K.; Wurpel, G. W. H.; Müller, M.; Bakker, H. J.; Bonn, M. Comment on "Vibrational Response of Hydrogen-Bonded Interfacial Water is Dominated by Intramolecular Coupling" Reply. *Phys. Rev. Lett.* **2008**, *101*, 139402.
(20) Tian, C. S.; Shen, Y. R. Comment on "Vibrational Response of Hydrogen-Bonded Interfacial Water is Dominated by Intramolecular Coupling. *Phys. Rev. Lett.* **2008**, *101*, 139401.
(21) Ishiyama, T.; Takahashi, H.; Morita, A. Vibrational Spectrum at a Water Surface: a Hybrid Quantum Mechanics/Molecular Mechanics Molecular Dynamics Approach. *J. Phys.: Condens. Matter* **2012**, *24*, 124107.
(22) Pieniazek, P. A.; Tainter, C. J.; Skinner, J. L. Surface of Liquid Water: Three-Body Interaction and Vibrational Sum-Frequency Spectroscopy. *J. Am. Chem. Soc.* **2012**, *133*, 10360−10363.
(23) Du, Q.; Freysz, E.; Shen, Y. R. Surface Vibrational Spectroscopic Studies of Hydrogen-Bonding and Hydrophobicity. *Science* **1994**, *264*, 826−828.
(24) Scatena, L. F.; Brown, M. G.; Richmond, G. L. Water at Hydrophobic Surfaces: Weak Hydrogen Bonding and Strong Orientation Effects. *Science* **2001**, *292*, 908−912.
(25) McFearin, C. L.; Beaman, D. K.; Moore, F. G.; Richmond, G. L. From Franklin to Today: Toward a Molecular Level Understanding of Bonding and Adsorption at the Oil−Water Interface. *J. Phys. Chem. C* **2009**, *113*, 1171−1188.
(26) Davis, J. G.; Gierszal, K. P.; Wang, P.; Ben-Amotz, D. Water Structural Transformation at Molecular Hydrophobic Interfaces. *Nature* **2012**, *491*, 582−585.
(27) Pratt, L. R.; Chandler, D. Theory of the Hydrophobic Effect. *J. Chem. Phys.* **1977**, *67*, 3683−3704.
(28) Pratt, L. R.; Pohorille, A. Theory of Hydrophobicity—Transient Cavities in Molecular Liquids. *Proc. Natl. Acad. Sci. U.S.A.* **1992**, *89*, 2995−2999.
(29) Lum, K.; Chandler, D.; Weeks, J. D. Hydrophobicity at Small and Large Length Scales. *J. Phys. Chem. B* **1999**, *103*, 4570−4577.
(30) Ashbaugh, H. S.; Pratt, L. R. Colloquium: Scaled Particle Theory and the Length Scales of Hydrophobicity. *Rev. Mod. Phys.* **2006**, *78*, 159−178.
(31) Sarupria, S.; Garde, S. Quantifying Water Density Fluctuations and Compressibility of Hydration Shells of Hydrophobic Solutes and Proteins. *Phys. Rev. Lett.* **2009**, *103*, 037803.

(32) Patel, A. J.; Varilly, P.; Chandler, D. Fluctuations of Water near Extended Hydrophobic and Hydrophilic Surfaces. *J. Phys. Chem. B* **2010**, *114*, 1632−1637.
(33) Patel, A. J.; Varilly, P.; Jamadagni, S. N.; Hagan, M. F.; Chandler, D.; Garde, S. Sitting at the Edge: How Biomolecules Use Hydrophobicity To Tune Their Interactions and Function. *J. Phys. Chem. B* **2012**, *116*, 2498−2503.
(34) Hsieh, C.-S.; Campen, R. K.; Verde, A. C. V.; Bolhuis, P.; Nienhuys, H.-K.; Bonn, M. Ultrafast Reorientation of Dangling OH Groups at the Air−Water Interface Using Femtosecond Vibrational Spectroscopy. *Phys. Rev. Lett.* **2011**, *107*, 116102.
(35) Vila Verde, A.; Bolhuis, P. G.; Campen, R. K. Statics and Dynamics of Free and Hydrogen-Bonded OH Groups at the Air/Water Interface. *J. Phys. Chem. B* **2012**, *116*, 9467−9481.
(36) Stiopkin, I. V.; Jayathilake, H. D.; Weeraman, C.; Benderskii, A. V. Temporal Effects on Spectroscopic Line Shapes, Resolution, and Sensitivity of the Broad-Band Sum Frequency Generation. *J. Chem. Phys.* **2010**, *132*, 234503.
(37) Curtis, A. D.; Asplund, M. C.; Patterson, J. E. Use of Variable Time-Delay Sum-Frequency Generation for Improved Spectroscopic Analysis. *J. Phys. Chem. C* **2011**, *115*, 19303−19310.
(38) Curtis, A. D.; Burt, S. R.; Calchera, A. R.; Patterson, J. E. Limitations in the Analysis of Vibrational Sum-Frequency Spectra Arising from the Nonresonant Contribution. *J. Phys. Chem. C* **2011**, *115*, 11550−11559.
(39) Liu, D. F.; Ma, G.; Levering, L. M.; Allen, H. C. Vibrational Spectroscopy of Aqueous Sodium Halide Solutions and Air−Liquid Interfaces: Observation of Increased Interfacial Depth. *J. Phys. Chem. B* **2004**, *108*, 2252−2260.
(40) Mucha, M.; Frigato, T.; Levering, L. M.; Allen, H. C.; Tobias, D. J.; Dang, L. X.; Jungwirth, P. Unified Molecular Picture of the Surfaces of Aqueous Acid, Base, and Salt Solutions. *J. Phys. Chem. B* **2005**, *109*, 7617−7623.
(41) Rezus, Y. L. A.; Bakker, H. J. On the Orientational Relaxation of HDO in Liquid Water. *J. Chem. Phys.* **2005**, *123*, 114502.
(42) Denzler, D. N.; Hess, C.; Dudek, R.; Wagner, S.; Frischkorn, C.; Wolf, M.; Ertl, G. Interfacial Structure of Water on Ru(001) Investigated by Vibrational Spectroscopy. *Chem. Phys. Lett.* **2003**, *376*, 618−624.
(43) Weber, M. J. *Handbook of Optical Materials*; CRC Press: Boca Raton, Fl, 2010; Vol. *19*, Chapter 1.9.4.
(44) Phillips, J. C.; Braun, R.; Wang, W.; Gumbart, J.; Tajkhorshid, E.; Villa, E.; Chipot, C.; Skeel, R. D.; Kale, L.; Schulten, K. Scalable molecular dynamics with NAMD. *J. Comput. Chem.* **2005**, *26*, 1781−1802.
(45) Humphrey, W.; Dalke, A.; Schulten, K. VMD: Visual Molecular Dynamics. *J. Mol. Graph.* **1996**, *14*, 33−38.
(46) Berendsen, H. J. C.; Grigera, J. R.; Straatsma, T. P. The Missing Term in Effective Pair Potentials. *J. Phys. Chem.* **1987**, *91*, 6269−6271.
(47) Lamoureux, G.; Harder, E.; Vorobyov, I. V.; Roux, B.; MacKerell, A. D., Jr. A Polarizable Model of Water for Molecular Dynamics Simulations of Biomolecules. *Chem. Phys. Lett.* **2006**, *418*, 245−249.
(48) Lawrence, C. P.; Skinner, J. L. Flexible TIP4P Model for Molecular Dynamics Simulation of Liquid Water. *Chem. Phys. Lett.* **2003**, *372*, 842−847.
(49) Rey, R.; Hynes, J. T. Vibrational Energy Relaxation of HOD in Liquid D_2O. *J. Chem. Phys.* **1996**, *104*, 2356−2368.
(50) Schmidt, J. R.; Roberts, S. T.; Loparo, J. J.; Tokmakoff, A.; Fayer, M. D.; Skinner, J. L. Are Water Simulation Models Consistent with Steady-State and Ultrafast Vibrational Spectroscopy Experiments? *Chem. Phys.* **2007**, *341*, 143−157.
(51) Smit, B. Phase Diagrams of Lennard-Jones Fluids. *J. Chem. Phys.* **1992**, *96*, 8639−8640.
(52) Ismail, A. E.; Grest, G. S.; Stevens, M. J. Capillary Waves at the Liquid−Vapor Interface and the Surface Tension of Water. *J. Chem. Phys.* **2006**, *125*, 014702.
(53) Janeček, J. Long Range Corrections in Inhomogeneous Simulations. *J. Phys. Chem. B* **2006**, *110*, 6264−6269.
(54) Alejandre, J.; Tildesley, D. J.; Chapela, G. A. Molecular Dynamics Simulation of the Orthobaric Densities and Surface Tension of Water. *J. Chem. Phys.* **1995**, *102*, 4574−4583.
(55) Trokhymchuk, A.; Alejandre, J. Computer Simulations of Liquid/Vapor Interface in Lennard-Jones Fluids: Some Questions and Answers. *J. Chem. Phys.* **1999**, *111*, 8510−8523.
(56) Jiang, W.; Hardy, D. J.; Phillips, J. C.; MacKerell, A. D.; Schulten, K.; Roux, B. High-Performance Scalable Molecular Dynamics Simulations of a Polarizable Force Field Based on Classical Drude Oscillators in NAMD. *J. Phys. Chem. Lett.* **2010**, *2*, 87−92.
(57) Wood, W. W. In *Physics of Simple Liquids*; Temperley, H. N. V., Rowlinson, J. S., Rushbrooke, G. S., Eds.; North-Holland publishing Co.: Amsterdam, 1968; Chapter 5, pp 151−155.
(58) Chitra, R.; Yashonath, S. Estimation of Error in the Diffusion Coefficient from Molecular Dynamics Simulations. *J. Phys. Chem. B* **1997**, *101*, 5437−5445.
(59) Lambert, A. G.; Davies, P. B.; Neivandt, D. J. Implementing the Theory of Sum Frequency Generation Vibrational Spectroscopy: A Tutorial Review. *Appl. Spectrosc. Rev.* **2005**, *40*, 103−145.
(60) Heinz, T. F. In *Nonlinear Surface Electromagnetic Phenomena*; Ponrath, H. E., Stegeman, G. I., Eds.; Elsevier Science Publishers: Amsterdam, 1991; pp 353−416.
(61) Zhuang, X.; Miranda, P. B.; Kim, D.; Shen, Y. R. Mapping Molecular Orientation and Conformation at Interfaces by Surface Nonlinear Optics. *Phys. Rev. B* **1999**, *59*, 12632−12640.
(62) Wei, X.; Miranda, P. B.; Zhang, C.; Shen, Y. R. Sum-Frequency Spectroscopic Studies of Ice Interfaces. *Phys. Rev. B* **2002**, *66*, 13.
(63) Laaser, J. E.; Xiong, W.; Zanni, M. T. Time-Domain SFG Spectroscopy Using Mid-IR Pulse Shaping: Practical and Intrinsic Advantages. *J. Phys. Chem. B* **2011**, *115*, 2536−2546.
(64) Stiopkin, I. V.; Weeraman, C.; Pieniazek, P. A.; Shalhout, F. Y.; Skinner, J. L.; Benderskii, A. V. Hydrogen Bonding at the Water Surface Revealed by Isotopic Dilution Spectroscopy. *Nature* **2011**, *474*, 192−195.
(65) Walrafen, G. E.; Yang, W. H.; Chu, Y. C.; Hokmabadi, M. S. Raman OD-Stretching Overtone Spectra from Liquid D_2O between 22 and 152° C. *J. Phys. Chem.* **1996**, *100*, 1381−1391.
(66) Zhang, Z.; Piatkowski, L.; Bakker, H. J.; Bonn, M. Ultrafast Vibrational Energy Transfer at the Water/Air Interface Revealed by Two-Dimensional Surface Vibrational Spectroscopy. *Nat. Chem.* **2011**, *3*, 888−893.
(67) Netz, R. R.; Horinek, D. Progress in Modeling of Ion Effects at the Vapor/Water Interface. *Annu. Rev. Phys. Chem.* **2012**, *63*, 401−418.
(68) Chacón, E.; Tarazona, P.; Alejandre, J. The Intrinsic Structure of the Water Surface. *J. Chem. Phys.* **2006**, *125*, 014709.
(69) Willard, A. P.; Chandler, D. Instantaneous Liquid Interfaces. *J. Phys. Chem. B* **2010**, *114*, 1954−1958.